# The Bcl-2 homolog Nrz inhibits binding of IP3 to its receptor to control calcium signaling during zebrafish epiboly

Benjamin Bonneau, Adrien Nougarède, Julien Prudent, Nikolay Popgeorgiev, Nadine Peyriéras, Ruth Rimokh, Germain Gillet

# The Bcl-2 Homolog Nrz Inhibits Binding of $IP_3$ to Its Receptor to Control Calcium Signaling During Zebrafish Epiboly

**Benjamin Bonneau,[1] Adrien Nougarède,[1] Julien Prudent,[1] Nikolay Popgeorgiev,[1] Nadine Peyriéras,[2] Ruth Rimokh,[1] Germain Gillet[1]***

Members of the Bcl-2 protein family regulate mitochondrial membrane permeability and also localize to the endoplasmic reticulum where they control $Ca^{2+}$ homeostasis by interacting with inositol 1,4,5-trisphosphate ($IP_3$) receptors ($IP_3Rs$). In zebrafish, Bcl-2–like 10 (Nrz) is required for $Ca^{2+}$ signaling during epiboly and gastrulation. We characterized the mechanism by which Nrz controls $IP_3$-mediated $Ca^{2+}$ release during this process. We showed that Nrz was phosphorylated during early epiboly, and that in embryos in which Nrz was knocked down, reconstitution with Nrz bearing mutations designed to prevent its phosphorylation disrupted cyclic $Ca^{2+}$ transients and the assembly of the actin-myosin ring and led to epiboly arrest. In cultured cells, wild-type Nrz, but not Nrz with phosphomimetic muta-tions, interacted with the $IP_3$ binding domain of $IP_3R1$, inhibited binding of $IP_3$ to $IP_3R1$, and prevented histamine-induced increases in cytosolic $Ca^{2+}$. Collectively, these data suggest that Nrz phosphorylation is necessary for the generation of $IP_3$-mediated $Ca^{2+}$ transients and the formation of circumferential actin-myosin cables required for epiboly. Thus, in addition to their role in apoptosis, by tightly regulating $Ca^{2+}$ signaling, Bcl-2 family members participate in the cellular events associated with early vertebrate devel-opment, including cytoskeletal dynamics and cell movement.

## INTRODUCTION

The Bcl-2 protein family has both pro- and antiapoptotic functions, including the control of mitochondrial membrane permeability to cytochrome c, which leads to caspase activation (*1*). In addition, Bcl-2 proteins localize to the endoplasmic reticulum (ER) where they participate in $Ca^{2+}$ homeostasis by binding to the $Ca^{2+}$ channel, inositol 1,4,5-trisphosphate ($IP_3$) receptor ($IP_3R$) (*2*). $IP_3$ binding to $IP_3Rs$ promotes $Ca^{2+}$ efflux from the ER into the cytosol, a process known as $IP_3$-induced $Ca^{2+}$ release (IICR). $IP_3Rs$ are composed of five types of domains (*3*): the suppressor domain (SD), the $IP_3$-binding domain ($IP_3BD$), the modulatory and transducing domain (MTD), the channel-forming domain (CFD), and the coupling domain (CD). The SD and $IP_3BD$ mediate binding to $IP_3$, the MTD binds regulatory molecules that modify $IP_3R$ activity and transduces the signal from the $IP_3BD$ to the CFD, and the CD is implicated in $IP_3R$ tetramerization and channel opening (*4*). Bcl-2 inhibits IICR by interacting with the MTD (*5*), whereas Bcl-xL promotes $Ca^{2+}$ release at low concentrations of $IP_3$ by interacting with the CD (*6*).

$Ca^{2+}$ release through $IP_3Rs$ mediates many cellular and physiological processes, such as cell proliferation, differentiation, apoptosis, fertilization, and embryonic development (*7*). In the zebrafish embryo, $Ca^{2+}$ signaling plays a role in early stages of development (*8*). At the onset of the blastula stage, blastomeres that are in contact with the yolk release the contents of their cytoplasm into the yolk cell forming the yolk syncytial layer (YSL). At the end of blastulation, the embryo comprises blastomeres on top of the yolk cell, which contains the YSL. Before gastrulation, the blastomeres and the YSL begin to migrate from the animal to the vegetal pole in a process known as epiboly (*9*). In the YSL, $IP_3R$-dependent $Ca^{2+}$ signaling occurs at the onset of epiboly (*10*) and again once the blastomeres have passed the equator of the embryo (*11*). A contractile actin-myosin ring forms at the blastoderm margin (*12*) and is likely required for epiboly progression.

We recently demonstrated that the antiapoptotic protein Nrz, the zebrafish ortholog of Nrh-Bcl2l10, plays a crucial role in the progression of zebrafish epiboly. During early development, zygotic *nrz* is specifically expressed in the YSL, and knockdown of Nrz by morpholino (MO) injection results in epiboly arrest, constriction of the blastoderm margin, and detachment of the embryo from the yolk cell (*13*). This phenotype does not require caspase activity; instead, Nrz binds to $IP_3R1$ on the surface of the ER and decreases IICR (*14*). Knockdown of *nrz* increases the concentration of $Ca^{2+}$ at the blastoderm margin and promotes phosphorylation of myosin light chain (MLC) and premature formation of the circumferential actin-myosin ring, resulting in the detachment of blastomeres from the yolk (*14*).

Here, we investigated how Nrz regulates $Ca^{2+}$ signals in the YSL during epiboly. We demonstrated that Nrz interacted with the $IP_3BD$ of $IP_3R1$ and disrupted its binding to $IP_3$. Furthermore, we showed that phosphorylation of Nrz prevented this interaction and promoted $Ca^{2+}$ oscillations and formation of the actin-myosin ring during epiboly.

## RESULTS

### The BH4-BH1 region of Nrz is required to inhibit IICR

We previously demonstrated that Nrz interacts with $IP_3R1$ via its N-terminal Bcl-2 homology (BH) 4 domain (*14*). Other members of the Bcl-2 family, including Bcl-2 and Bcl-xL, interact with $IP_3R1$ (*5*, *6*) and control IICR. Although the BH4 domain of Bcl-2 is sufficient to suppress IICR (*15*), the BH4 domain of Bcl-xL is not (*16*). To determine whether the BH4 domain of Nrz was required for IICR inhibition, we fused the BH4 domain of Nrz to the ER-targeting sequence of cytochrome b5 (NrzBH4Cb5) (Fig. 1A)

[1]Université de Lyon, Centre de recherche en cancérologie de Lyon, U1052 INSERM, UMR CNRS 5286, Université Lyon I, Centre Léon Bérard, 28 rue Laennec, 69008 Lyon, France. [2]CNRS-MDAM, UPR 3294 and BioEmergences-IBiSA, Institut de Neurobiologie Alfred Fessard, Avenue de la Terrasse, 91198 Gif-sur-Yvette Cedex, France.
*Corresponding author. E-mail: germain.gillet@univ-lyon1.fr

and transiently overexpressed the fusion protein in HeLa cells. Similar to the Nrz BH4 domain that localizes in the cytoplasm (*14*) or full-length Nrz targeted to the ER (NrzCb5), NrzBH4Cb5 coimmunoprecipitated with endogenous $IP_3R1$ (Fig. 1B). To assess whether NrzBH4Cb5 affects IICR, we monitored changes in the concentration of cytosolic $Ca^{2+}$ using a $Ca^{2+}$-sensitive fluorescent dye. In human umbilical vein endothelial cells, histamine triggers $IP_3$ accumulation and increases cytosolic $Ca^{2+}$, which can be reversed by inhibition of protein kinase C (*17*). We found that treating HeLa cells with histamine induced a transient increase in the concentration of cytosolic $Ca^{2+}$ and that overexpression of NrzCb5, but not of NrzBH4Cb5, partially inhibited this effect (Fig. 1, C and D), suggesting that the BH4 domain is not sufficient to inhibit IICR.

Nrz contains a total of four BH domains, numbered BH4, BH3, BH1, and BH2, from the N to the C terminus (Fig. 1A). Thus, we asked whether longer N-terminal fragments of Nrz containing other BH domains could affect IICR. Consistent with the fact that the BH4 domain of Nrz mediates its interaction with $IP_3R1$, we found that all forms of C-terminally truncated Nrz coimmunoprecipitated with endogenous $IP_3R1$ (Fig. 1E). However, overexpression of the Nrz BH1, BH3, and BH4 domains (Nrz1-94Cb5) significantly reduced histamine-induced increased cytosolic $Ca^{2+}$, whereas overexpression of the Nrz BH3 and BH4 domains (Nrz1-67Cb5) did not (Fig. 1, F and G), suggesting that the BH1 domain is required for IICR.

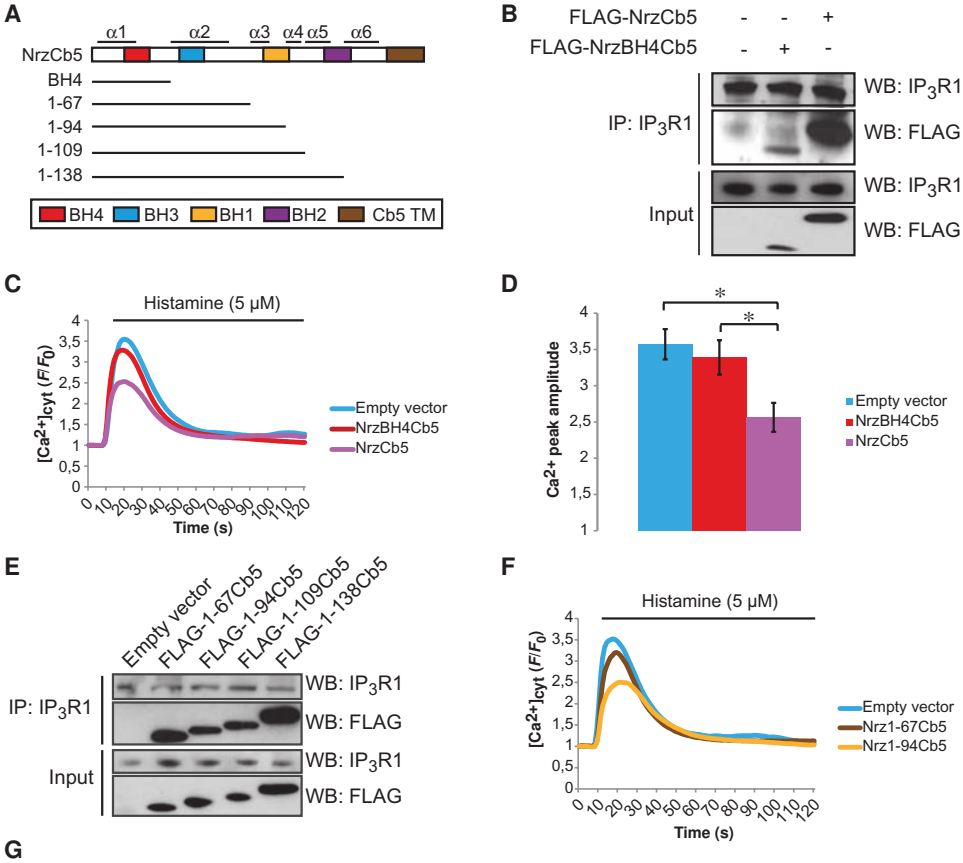


Fig. 1. Nrz requires its BH4-BH1 region to bind $IP_3R1$ and regulate IICR in HeLa cells. (A) Schematic of full-length Nrz and the Cb5 domain of cytochrome b. Lines and colored boxes represent α helices and BH domains, respectively. (B) Representative Western blot of immunoprecipitation (IP) between endogenous $IP_3R1$ and FLAG-NrzBH4 or FLAG-NrzCb5. $n = 3$. (C) Representative $Ca^{2+}$ response curve of cells stimulated with 5 μM histamine at the indicated times. Cells were transfected with empty vector, FLAG-NrzBH4Cb5, or FLAG-NrzCb5. (D) Histogram showing the mean amplitude (±SD) of the histamine-induced $Ca^{2+}$ peak. $n \geq 5$ fields from biological replicates. (E) Representative Western blot of IP between endogenous $IP_3R1$ and FLAG-tagged C-terminal Nrz deletion mutants. $n = 3$. (F) Representative $Ca^{2+}$ response curve of cells stimulated with 5 μM histamine at the indicated times. Cells were transfected with empty vector, FLAG-Nrz1-67Cb5, or FLAG-Nrz1-94Cb5. (G) Histogram showing the mean amplitude (±SD) of the histamine-induced $Ca^{2+}$ peak. $n \geq 5$ fields from biological replicates. *$P < 0.005$ (Mann-Whitney *U* test) for (D) and (G).

## Nrz inhibition of IICR is independent of its interaction with the proapoptotic protein Bax

The fact that the BH1 domain of Nrz was required for its interaction with $IP_3R1$ could mean that the ability of Nrz to inhibit IICR is related to its ability to bind proapoptotic members of the Bcl-2 family. The BH1 domain of Bcl-2 family proteins contains a conserved Asn-Try-Gly-Arg motif. Mutation of $Gly^{145}$ to Ala in Bcl-2 prevents its heterodimerization with the proapoptotic protein Bax (*18*). To test whether the analogous residue in Nrz mediated dimerization with Bax, we mutated $Gly^{85}$ to Ala in otherwise wild-type Nrz (NrzG85A). We found that full-length wild-type Nrz, but not NrzG85A or Nrz1-94, coimmunoprecipitated endogenous Bax (Fig. 2A) and reduced the abundance of cleaved poly (adenosine 5′-diphosphate–ribose) polymerase (PARP) induced by overexpression of Bax in HeLa cells (Fig. 2B), suggesting that the $Gly^{85}$ residue in the BH1 domain is important for Nrz-dependent inhibition of Bax-mediated apoptosis. Thus, we asked whether $Gly^{85}$ was required for Nrz to inhibit IICR. We fused the NrzG85A to the ER-targeting Cb5 domain (NrzG85ACb5) and expressed it in HeLa cells. We found that NrzG85ACb5 significantly reduced histamine-induced increases in cytosolic $Ca^{2+}$ (Fig. 2, C and D). Collectively, these results suggest that the function of Nrz to inhibit IICR is most likely independent of binding to Bax.

## Nrz binds to the $IP_3BD$ of $zIP_3R1$

The BH4 domain of several antiapoptotic Bcl-2 family proteins, including Bcl-2 and Bcl-xL, interacts with either the MTD or CD of $IP_3R1$, which is determined by the primary sequence of the BH4 domains (*5*, *6*, *16*, *19*, *20*). The primary sequence of the Nrz BH4 domain differs considerably from those of zBcl-2 and zBcl-xL (fig.

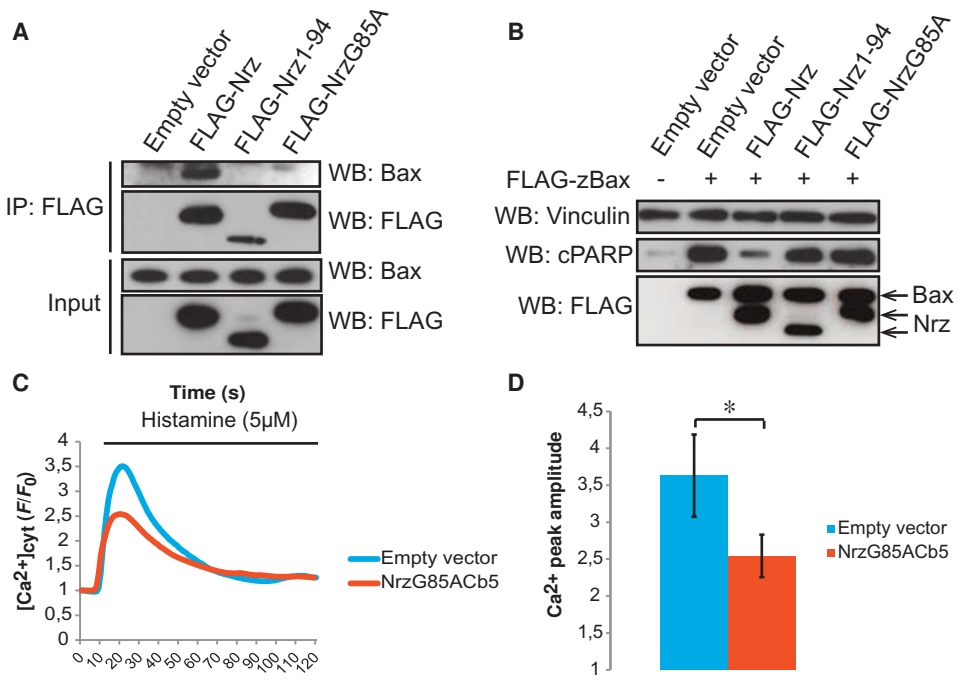


Fig. 2. Nrz regulates IICR in HeLa cells independent of its interaction with Bax. (**A**) Representative Western blot of IP between endogenous Bax and FLAG-tagged Nrz, Nrz1-94, or NrzG85A. $n = 3$. (**B**) Representative Western blot of cleaved PARP (cPARP) in cells transiently expressing zBax (zebrafish Bax) and FLAG-tagged full-length Nrz, Nrz1-94, or NrzG85A. $n = 3$. (**C**) Representative $Ca^{2+}$ response curve of cells stimulated with 5 μM histamine at the indicated times. Cells were transfected with empty vector or FLAG-NrzG85ACb5. (**D**) Histogram showing mean amplitude (±SD) of the histamine-induced $Ca^{2+}$ peak. $n \geq 5$ fields from biological replicates. $^*P < 0.005$ (Mann-Whitney *U* test).

S1). To determine which domain of Nrz interacts with $IP_3R1$, we expressed fragments of zebrafish $IP_3R1$ ($zIP_3R1$) (Fig. 3A) in HeLa cells. We found that the $IP_3BD$, but not the SD, MTDs, or CD, of $zIP_3R1$ coimmunoprecipitated NrzCb5 (Fig. 3B) but not NrzCb5 lacking the BH4 domain (NrzΔBH4Cb5) (fig. S2), suggesting that the interaction between Nrz and $IP_3R1$ is mediated by the specific binding of the $IP_3BD$ of $IP_3R1$ to the BH4 domain of Nrz.

## Nrz binds outside the $IP_3$ binding pocket of $IP_3R1$

A group of residues in the $IP_3BD$ form a positively charged pocket in the $IP_3$-binding site (*21*). In mouse $IP_3R1$, point mutations in these residues abolish the binding of both $IP_3$ (*21*) and IRBIT ($IP_3R$-binding protein released with $IP_3$), a competitive inhibitor of $IP_3$ (*22*, *23*). These residues are conserved in zebrafish; therefore, we asked whether they were required for binding to Nrz. Individual mutations to each of the corresponding amino acids did not affect the ability of the $IP_3BD$ of $zIP_3R1$ to coimmunoprecipitate NrzCb5 (Fig. 3C) when coexpressed in HeLa cells, suggesting that, unlike IRBIT, Nrz does not act as a competitive inhibitor of $IP_3$ binding to $IP_3R1$.

To identify which residues could govern the interaction of $IP_3R1$ and Nrz, we performed molecular docking simulation between the $IP_3BD$ of mouse $IP_3R1$ [Protein Data Bank (PDB): 1N4K] and the BH4 domain of Nrz (Fig. 3D). This analysis suggested that Nrz interacts with $IP_3R1$ outside of the $IP_3$ binding pocket, consistent with the mutational analysis (Fig. 3C), and identified three residues in $IP_3R1$ that could mediate its interaction with Nrz. We mutated the corresponding residues in $zIP_3R1$ ($Glu^{255}$, $Glu^{410}$, and $Tyr^{576}$) and performed coimmunoprecipitation experiments in HeLa cells. We found that E225A prevented the interaction of NrzCb5 with the $IP_3BD$ (Fig. 3E), indicating that $Glu^{255}$ of $zIP_3R1$ was critical for binding to Nrz. Analysis of docking solutions also indicated that the interaction of Nrz and $IP_3R1$ may depend on the interaction between $zIP_3R1$ $Glu^{255}$ and $Cys^{20}$ of Nrz. Analysis of primary sequence alignments demonstrated that $Cys^{20}$ is highly conserved across Nrz orthologs (fig. S3), suggesting that this residue could be important for binding between Nrz and $zIP_3R1$ and that this interaction could be evolutionarily conserved.

## Nrz prevents $IP_3$ from binding to $IP_3R1$

We found that Nrz inhibits IICR and binds to the $IP_3BD$ of $IP_3R1$, suggesting that it could interfere with $IP_3$ binding to $IP_3R1$. We verified that Nrz does not affect the steady-state concentration of $Ca^{2+}$ in the ER. In HeLa cells, expression of NrzCb5 did not affect increased cytosolic $Ca^{2+}$ caused by treatment with thapsigargin (fig. S4), which inhibits the sarco-endoplasmic reticulum $Ca^{2+}$ adenosine triphosphatase (ATPase) and thereby flushes $Ca^{2+}$ from the ER (*24*).

To test whether Nrz could prevent binding of $IP_3$ to $IP_3R1$ to inhibit IICR, we used the $IP_3R$-based $IP_3$ sensor (IRIS), which contains the $IP_3BD$ flanked by enhanced cyan fluorescent protein (ECFP) and the yellow fluorescent protein Venus. When $IP_3$ binds to IRIS, it induces a conformational change in the $IP_3BD$ that decreases fluorescence resonance energy transfer (FRET) from ECFP to Venus (*25*). Treating HeLa cells expressing IRIS with histamine induced a rapid increase in the ratio (*R*) between ECFP and Venus fluorescence intensities, indicating reduced FRET (Fig. 4A). Transient overexpression of full-length wild-type Nrz or Nrz1-94, but not NrzBH4 or NrzΔBH4, prevented histamine-induced changes in the IRIS FRET ratio (Fig. 4, A and B). We also directly assessed the binding of $IP_3$ to $IP_3R1$ using fluorescence polarization (*26*) to measure the interaction between $IP_3$ covalently bound to fluorescein isothiocyanate ($IP_3$-FITC) and a recombinant protein composed of the SD and $IP_3BD$ of $IP_3R1$ ($IP_3R1$-NTD). When we incubated $IP_3$-FITC with $IP_3R1$-NTD in the presence of recombinant Nrz, we found that Nrz reduced fluorescence polarization in a concentration-dependent manner (half-maximal inhibitory concentration, $2.96 \times 10^{-8} \pm 1.77 \times 10^{-8}$ M) (Fig. 3C). Collectively, these results demonstrate that Nrz inhibits the binding of $IP_3$ to $IP_3R1$.

## Phosphorylation of Nrz inhibits its interaction with $IP_3R1$

We hypothesized that the interaction between endogenous Nrz and $IP_3R1$ could be regulated by signal transduction mechanisms such as phosphorylation. Phosphorylation of Bcl-2 on a Thr and two Ser residues in the loop between its BH4 and BH3 domains increases $Ca^{2+}$ release from the ER (*27*). Similar to Bcl-2, Nrz has a Thr and two Ser residues in the loop between the BH4 and BH3 domains (Fig. 5A) that could be phosphorylated. We mutated these three residues to generate phosphomimetic (T26D, S29D, S31D, NrzDDD) and nonphosphorylatable (T26A, S29A, S31A,

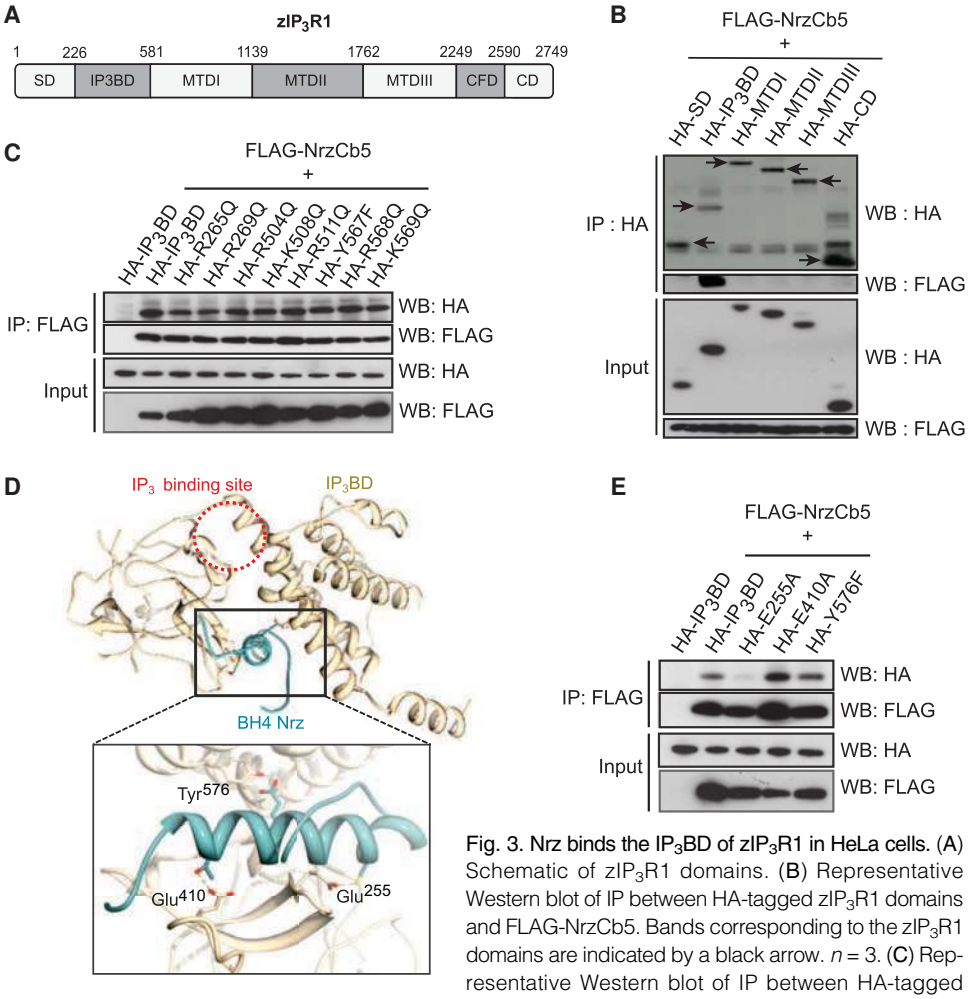


Fig. 3. Nrz binds the $IP_3BD$ of $zIP_3R1$ in HeLa cells. (**A**) Schematic of $zIP_3R1$ domains. (**B**) Representative Western blot of IP between HA-tagged $zIP_3R1$ domains and FLAG-NrzCb5. Bands corresponding to the $zIP_3R1$ domains are indicated by a black arrow. $n = 3$. (**C**) Representative Western blot of IP between HA-tagged $IP_3BD$ or $IP_3BD$ binding site mutants and FLAG-NrzCb5. $n = 3$. (**D**) Docking model of the BH4 domain of Nrz (modeled by multi-template homology with Phyre[2]) binding to the $IP_3BD$ of mouse $IP_3R1$ (PDB: 1N4K). The red dashed circle represents the $IP_3$ binding site. (**E**) Representative Western blot of IP between HA-tagged $IP_3BD$ domain or $IP_3BD$ mutants (E255A, E410A, Y576F) and FLAG-NrzCb5. $n = 3$.

NrzAAA) amino acid versions of Nrz. When transiently expressed in HeLa cells, NrzAAACb5, but not NrzDDDCb5, significantly decreased histamine-induced increased cytosolic $Ca^{2+}$ (Fig. 5, B and C). Moreover, NrzAAACb5, but not NrzDDDCb5, coimmunoprecipitated the $IP_3BD$ of $IP_3R1$ (Fig. 5D). To identify which of these three amino acids was important for Nrz interaction with $IP_3R1$, we generated single and double mutants at each position. We found that Nrz mutants containing S31D did not coimmunoprecipitate the $IP_3BD$ of $IP_3R1$ (Fig. 5E), suggesting that $Ser^{31}$ phosphorylation by an unknown kinase could play a critical role in inhibiting the interaction between Nrz and $IP_3R1$ and promoting IICR.

## Domains of Nrz required for the inhibition of IICR are also required for zebrafish epiboly

We previously reported that Nrz knockdown by antisense MO injection results in the constriction of the blastoderm margin and the detachment of the embryo from the yolk cell during epiboly (*13*). The injection of *nrz* MO induces a robust increase in cytosolic $Ca^{2+}$ and embryonic lethality, which can be prevented by co-injecting mRNA encoding NrzCb5 but not NrzΔBH4Cb5 (*14*). Here, we found that both the BH4 and BH1 domains of Nrz were required to inhibit IICR in HeLa cells (Fig. 1). Therefore, we tested whether these domains were sufficient to reverse the phenotype induced by *nrz* MO injection. We co-injected embryos with *nrz* MO and in vitro–synthesized mRNA encoding various truncated forms of Nrz and monitored the percentage of embryos showing abnormal margin constriction during epiboly (Fig. 6A). Co-injection of *nrzbh4cb5* did not prevent epiboly defects induced by *nrz* MO (Fig. 6, A and B), consistent with the observation that the BH4 domain was not sufficient to reduce IICR in HeLa cells. Moreover, co-injection of *nrz1-94cb5*, but not of *nrz1-67cb5*, also prevented epiboly defects induced by *nrz* MO (Fig. 6C), demonstrating a requirement for the BH1 domain of Nrz in this process. We also found that the ability of Nrz to prevent IICR was independent of its ability to bind to Bax in HeLa cells (Fig. 2C). Similarly, co-injection of *nrzG85A*, which encodes a form of Nrz that does not bind Bax (Fig. 2A), prevented epiboly defects induced by *nrz* MO (Fig. 6D). Finally, we found that Nrz phosphorylation could impair its interaction with $IP_3R1$ in HeLa cells (Fig. 5D). In zebrafish, co-injection of *nrz* MO with *nrzAAAcb5*, but not *nrzDDDcb5*, reduced the percentage of embryos with epiboly defects induced by *nrz* MO (Fig. 6E). Thus, the domains and residues of Nrz required to inhibit IICR in cultured cells are also required for zebrafish epiboly.

## Phosphorylation of Nrz enables $Ca^{2+}$ signaling, actin-myosin ring formation, and epiboly

During epiboly, $IP_3$-dependent cyclic increases in cytosolic $Ca^{2+}$ concentration, referred to as $Ca^{2+}$ waves, occur in the YSL (*10*), where *nrz* is expressed (*13*). Because Nrz inhibits $IP_3$ binding to $IP_3R1$ in HeLa cells (Fig. 4, A to C), we hypothesized that Nrz activity is negatively regulated to enable the generation of $Ca^{2+}$ waves. In HeLa cells, we found that mutants of Nrz that mimic phosphorylated Thr and Ser do not bind to $IP_3R1$ (Fig. 5D) or inhibit IICR (Fig. 5C). To examine whether Nrz is phosphorylated during epiboly in vivo, we injected *nrzcb5* mRNA and immunoprecipitated NrzCb5 from ER fractions prepared from the YSL of embryos at different developmental stages. Western blot analysis revealed that Nrz Ser phosphorylation was barely detectable before the onset of epiboly and increased robustly by 30% epiboly (Fig. 7A), suggesting that Nrz phosphorylation could be important to enable $IP_3$-dependent $Ca^{2+}$ signaling in vivo during this process.

We tested whether replacing endogenous Nrz with a nonphosphorylatable form of Nrz could disrupt $Ca^{2+}$ signaling. In wild-type embryos injected at the 128-cell stage with a $Ca^{2+}$-sensitive dye, we observed cyclic $Ca^{2+}$ waves in the YSL at 30% epiboly (Fig. 7, B to E, and movie S1). To evaluate the contribution of Nrz phosphorylation to the generation of these $Ca^{2+}$ waves, we co-injected *nrz* MO and *nrzAAAcb5* or *nrzcb5*. We found that *nrzcb5*, but not *nrzAAAcb5*, restored normal $Ca^{2+}$ waves in the absence of endogenous

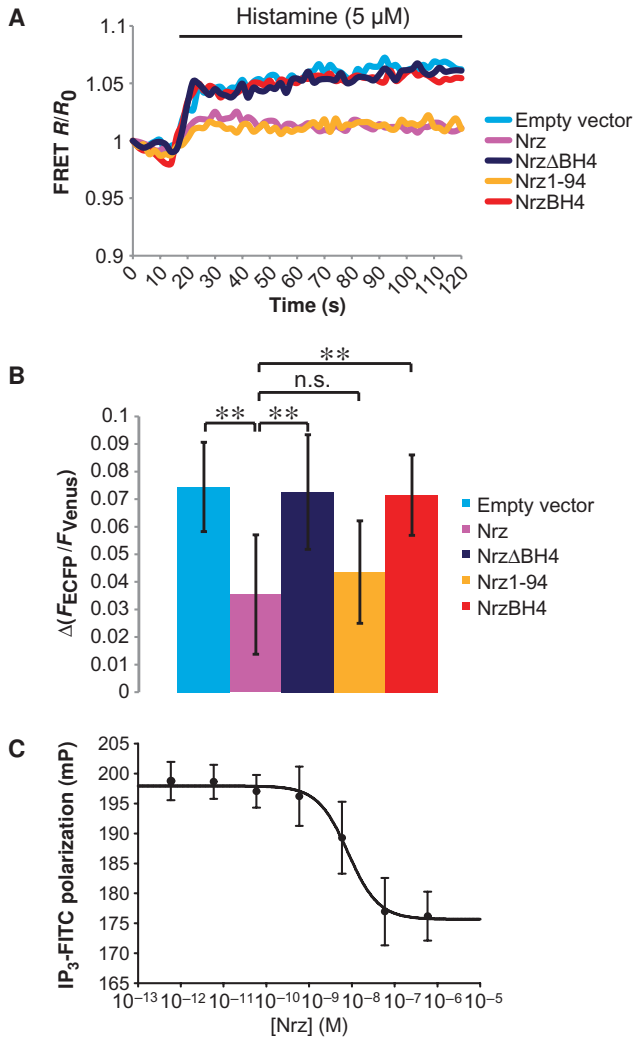


Fig. 4. Nrz prevents $IP_3$ binding to $IP_3R1$. (**A**) Representative curve of the FRET signal change of IRIS in HeLa cells stimulated with 5 μM histamine and expressing the indicated proteins. The FRET signal was calculated as the ratio (*R*) of fluorescence emission of ECFP to fluorescence emission of Venus with excitation at 405 nm. (**B**) Histogram showing the mean FRET signal change (±SD) induced by histamine stimulation. *n* = 30 cells from at least 3 biological replicates. $^{**}P < 0.0001$ (Mann-Whitney *U* test); n.s., nonsignificant ($P > 0.1$). (**C**) Curve showing the mean fluorescence polarization (±SD) of $IP_3$-FITC in the presence of $IP_3R1$ NTD and the indicated concentration of recombinant Nrz protein. *n* = 3 independent triplicate measurements.

Nrz (Fig. 7, B to E, and movies S2 and S3), suggesting that the phosphorylation of Nrz enables the generation of YSL $Ca^{2+}$ waves at the beginning of epiboly.

An actin-myosin ring forms at the blastoderm margin in zebrafish embryos at 40% epiboly, and localized disruption of actin in the YSL at 60% epiboly delays cell movements associated with epiboly progression (*12*). Similarly, treating zebrafish embryos at 50% epiboly with cytochalasin B, which inhibits actin network formation, or with a $Ca^{2+}$ chelator disrupts actin ring formation and epiboly (*28*), suggesting that $Ca^{2+}$ waves are important for the formation of the actin-myosin ring. Given that *nrzAAAcb5* disrupted $Ca^{2+}$ waves when co-injected with *nrz* MO, we examined the formation of the actin-myosin ring. Co-injection of *nrz* MO with *nrzAAAcb5*, but not *nrzcb5* or *nrz* MO injection alone, reduced F-actin staining at the blastoderm margin at 50% epiboly (Fig. 8, A and B), suggesting that the expression of nonphosphorylatable Nrz inhibits YSL $Ca^{2+}$ dynamics and thereby disrupts the formation of the actin-myosin ring.

The above data suggested that the phosphorylation of Nrz could be important for epiboly progression. In embryos injected with *nrz* MO, co-injection of *nrzAAAcb5*, but not of *nrzcb5*, resulted in epiboly delay (Fig. 8C) or arrest (Fig. 8D). Collectively, these results suggest that by 50% epiboly, endogenous Nrz is mostly phosphorylated and cannot bind to $IP_3R1$ and is thus permissive to $Ca^{2+}$ signaling required for actin assembly and contractility.

## DISCUSSION

We found that Nrz binds outside the $IP_3$ binding site on the $IP_3BD$ of $IP_3R1$ and prevents $IP_3$ binding, revealing a new regulatory mechanism for $IP_3Rs$ by Bcl-2–related proteins. Bcl-2 reduces $Ca^{2+}$ release by interacting with the MTD of $IP_3R1$ (*5*, *15*), and Bcl-xL sensitizes $IP_3R1$ to low $IP_3$ concentrations by interacting with the CD (*6*). The differential binding of Bcl-2 proteins to various domains of $IP_3R1$ may be determined by divergent amino acid sequences in the BH4 domains (*16*, *20*). Here, we found that the BH4 domain of Nrz was sufficient for it to interact with $IP_3R1$, suggesting that residues within this domain could be critical for determining the interaction with the $IP_3BD$. Molecular docking simulation identified a conserved Cys ($Cys^{20}$ in Nrz) as a potential factor in mitigating the binding of Nrz to the $IP_3BD$ of $IP_3R1$. We found that $Glu^{255}$ of $zIP_3R1$ most likely contacts Nrz $Cys^{20}$ and is essential for binding between these proteins. Whether Nrz $Cys^{20}$ is required to bind $IP_3R1$ and whether analogous residues confer specificity of binding of Bcl-2 family and other proteins to $IP_3BDs$ remain to be determined.

Several proteins interact with the $IP_3BD$ or decrease $IP_3$ binding to the $IP_3R1$. Beclin-1 binds to the $IP_3BD$ of $IP_3R1$, but Beclin-1 knockdown has no effect on $Ca^{2+}$ homeostasis (*29*). Sodium-potassium ATPase binds to the $IP_3BD$ of $IP_3R1$ (*30*) and promotes $Ca^{2+}$ release in the absence $IP_3$ (*31*). Carbonic anhydrase–related protein (CARP) inhibits $IP_3$ binding to $IP_3R1$ by reducing the affinity of the receptor for $IP_3$ (*32*). CARP interacts with the MTD of $IP_3R1$ (*32*), suggesting that Nrz and CARP act by distinct mechanisms. IRBIT binds the $IP_3BD$ of $IP_3R1$ and directly competes with $IP_3$ for binding to its receptor (*22*, *23*). We found that mutations in residues of $IP_3R1$ required for interaction with IRBIT and $IP_3$ were not required for binding to Nrz, suggesting that Nrz and IRBIT act by distinct mechanisms to inhibit $IP_3R1$. The Nrz BH4 domain binds outside the $IP_3$ binding site of $IP_3R1$, and the inhibition of IICR by Nrz requires the 94 most N-terminal amino acids including the BH4, BH3, and BH1 domains. The BH4 and BH3 domains combined were not sufficient to inhibit IICR without the BH1 domain, despite still being able to bind to $IP_3R1$. These findings imply that Nrz is an allosteric inhibitor. Binding of Nrz could produce a conformational change in the $IP_3BD$ of $IP_3R1$ that decreases the affinity of the $IP_3$ binding site for $IP_3$. Alternatively, Nrz, potentially involving its BH1 domain, could hinder access of $IP_3$ to the $IP_3$ binding site on $IP_3R1$ without direct competition for key residues.

The mutation of putative phosphorylated residues to phosphomimetic amino acids in Nrz prevented its ability to inhibit IICR and bind $IP_3R1$. Mutation of analogous residues in Bcl-2 to nonphosphorylatable amino acids enhances its ability to reduce $Ca^{2+}$ release from the ER (*27*). However, this effect is indirect. Phosphorylation of Bcl-2 reduces its interactions with proapoptotic proteins, such as Bax, which increases ER $Ca^{2+}$ content by reducing the $Ca^{2+}$ leak (*33*). Nrz did not alter basal ER $Ca^{2+}$

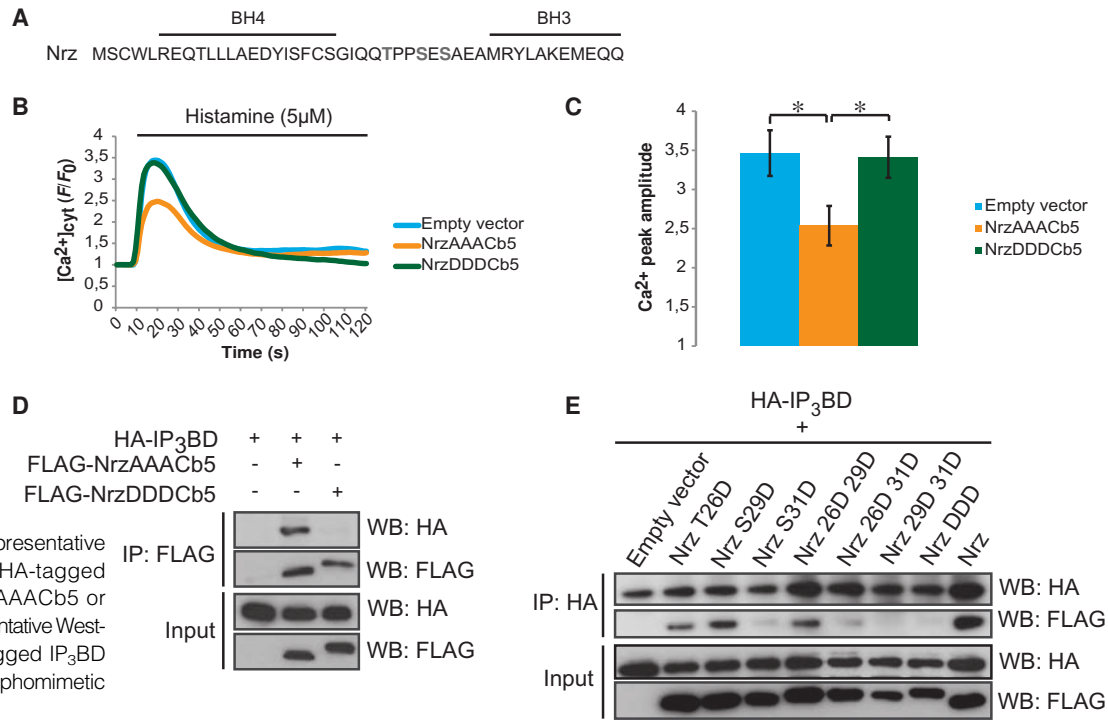


Fig. 5. Phosphomimetic mutant Nrz does not bind $IP_3R1$ or inhibit IICR in HeLa cells. (A) Primary sequence of the Nrz protein including the BH4 and BH3 domains. Putative phospho-serines and phospho-threonine are shown in red. (B) Representative $Ca^{2+}$ response curve of cells stimulated with 5 µM histamine at the indicated times. Cells were transfected with empty vector, FLAG-NrzAAACb5, or FLAG-NrzDDDCb5. (C) Histogram showing the mean amplitude (±SD) of the histamine-induced $Ca^{2+}$ peak. $n \geq 5$ fields from biological replicates. $^*P < 0.005$ (Mann-Whitney $U$ test). (D) Representative Western blot of IP between HA-tagged $IP_3BD$ and FLAG-tagged NrzAAACb5 or NrzDDDCb5. $n = 3$. (E) Representative Western blot of IP between HA-tagged $IP_3BD$ and FLAG-tagged Nrz or phosphomimetic Nrz mutants.

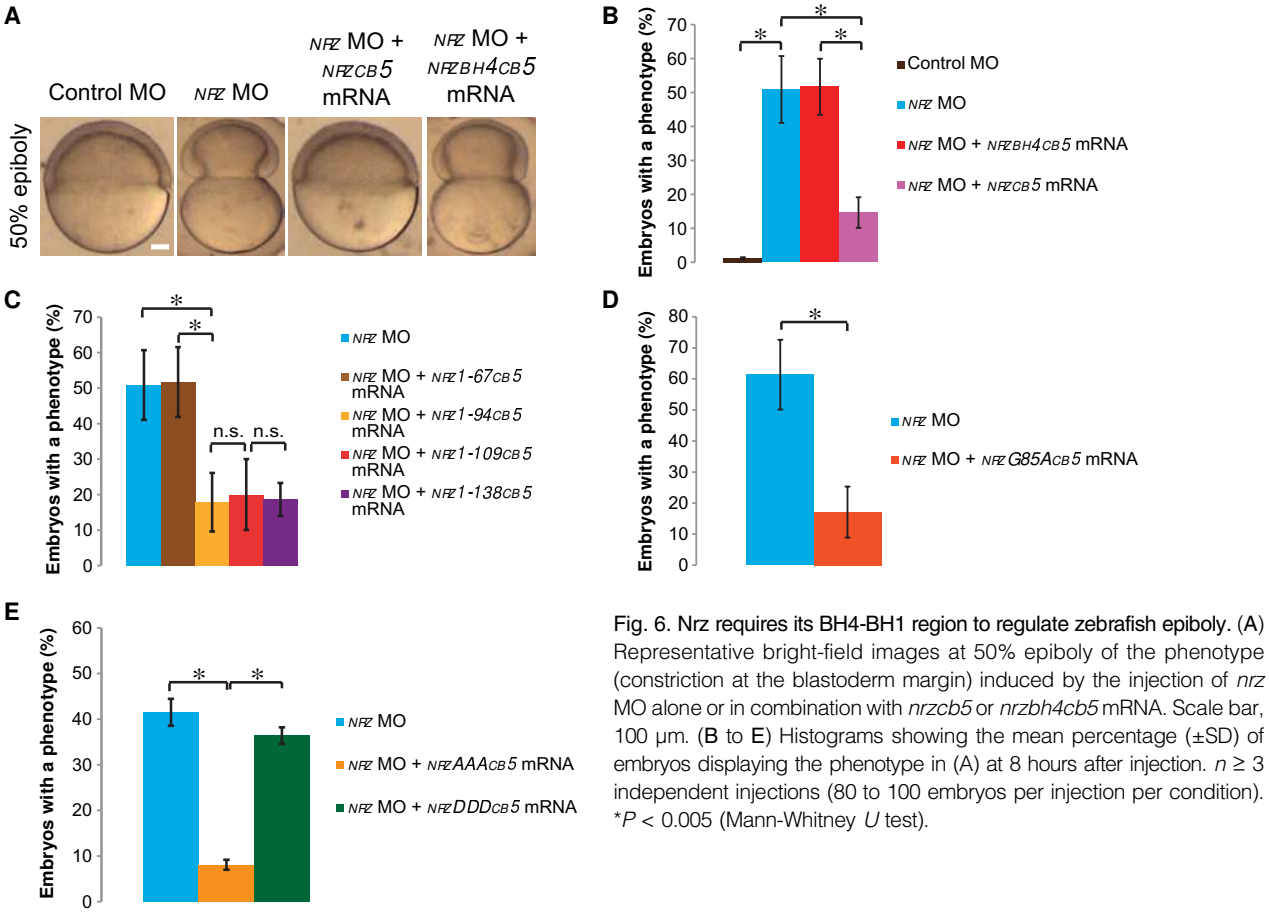


Fig. 6. Nrz requires its BH4-BH1 region to regulate zebrafish epiboly. (A) Representative bright-field images at 50% epiboly of the phenotype (constriction at the blastoderm margin) induced by the injection of *nrz* MO alone or in combination with *nrzcb5* or *nrzbh4cb5* mRNA. Scale bar, 100 µm. (B to E) Histograms showing the mean percentage (±SD) of embryos displaying the phenotype in (A) at 8 hours after injection. $n \geq 3$ independent injections (80 to 100 embryos per injection per condition). $^*P < 0.005$ (Mann-Whitney $U$ test).

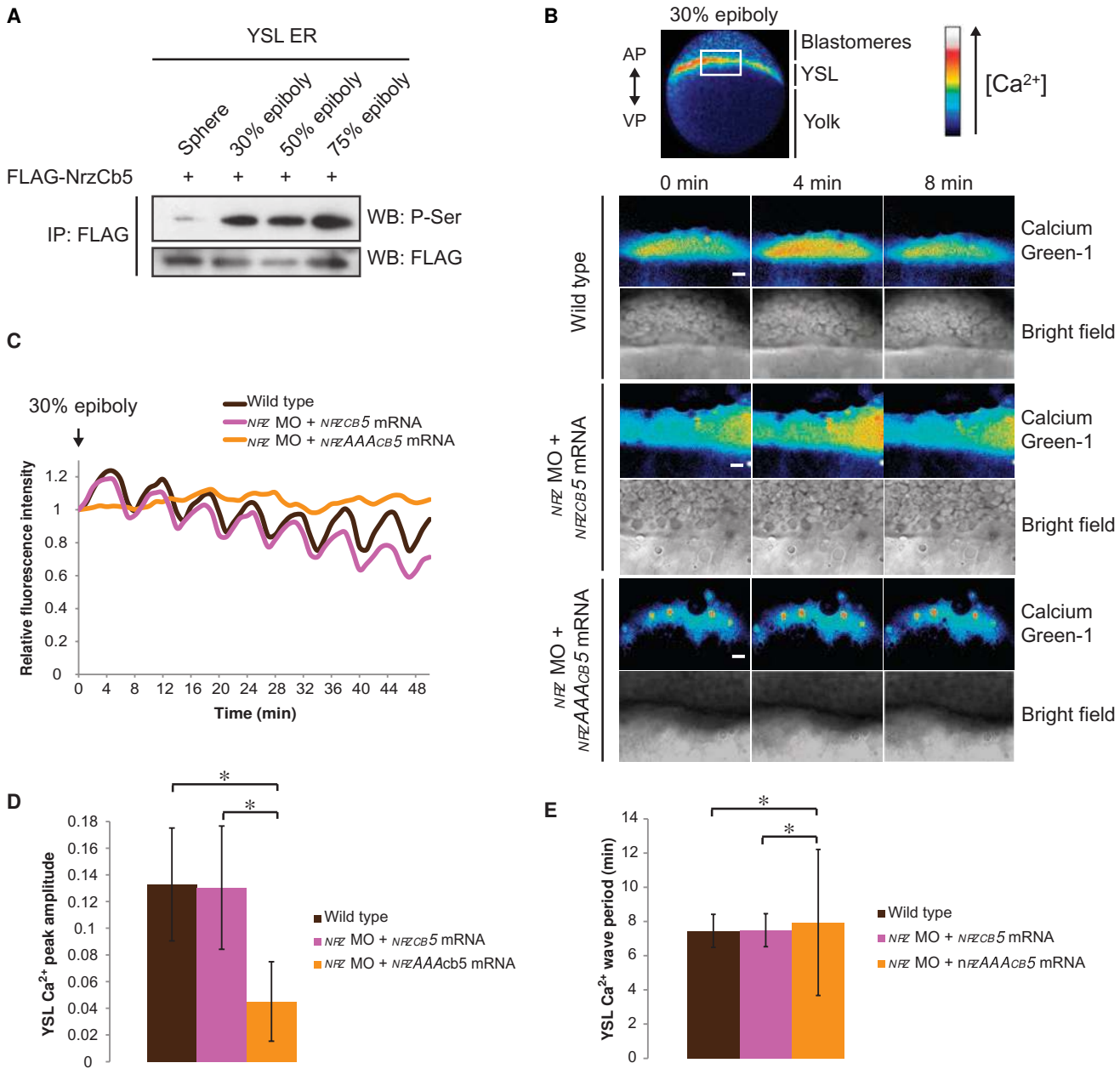


Fig. 7. Nrz phosphorylation is required for generation of cyclic $Ca^{2+}$ waves in the YSL. (**A**) Representative Western blot of IP for FLAG-NrzCb5 from ER of YSL cells isolated from embryos at the indicated stages. $n = 3$. (**B**) $Ca^{2+}$ concentration ($[Ca^{2+}]$) in the external YSL of uninjected wild-type embryos or embryos injected with *nrz* MO and *nrzcb5* or *nrzAAAcb5* mRNAs. Scale bars, 20 μm. (**C**) Representative graph of the $[Ca^{2+}]$ variation shown in (B). (**D** and **E**) Histograms showing the amplitude (D) or period (E) (mean ± SD) of YSL $[Ca^{2+}]$ as in (C). *$P < 0.005$ (Mann-Whitney *U* test). $n \geq 6$ embryos per condition.

concentration, and inhibition of IICR by Nrz did not require interaction with Bax. Moreover, phosphomimetic mutations in Nrz prevented interaction with the $IP_3BD$ of $IP_3R1$, suggesting that Nrz acts directly on $IP_3R1$-dependent $Ca^{2+}$ release in a manner that depends on Nrz phosphorylation.

We found that Nrz was phosphorylated during early zebrafish epiboly, a process that requires $Ca^{2+}$ signaling (*28*), and expression of Nrz with nonphosphorylatable amino acids suppressed cyclic $Ca^{2+}$ waves at the beginning of epiboly, compromised actin-myosin ring formation at the blastoderm margin, and delayed or disrupted epiboly. $Ca^{2+}$ waves begin at the time when the actin-myosin ring is formed (*12*, *28*), and our data are consistent with the fact that Nrz must be inhibited to enable this process. We observed that the period of $Ca^{2+}$ waves in the YSL was about 7 min. During myofibrillogenesis, actin-myosin network assembly is regulated by $Ca^{2+}$ transients with a similar period (*34*, *35*). At the blastoderm margin, actin associates with phospho–myosin-II (*36*). We previously demonstrated that increased cytosolic $Ca^{2+}$ concentrations in embryos injected with *nrz* MO promotes MLC phosphorylation, which leads to premature actin-myosin ring formation at 30% epiboly (*14*). Thus, $Ca^{2+}$

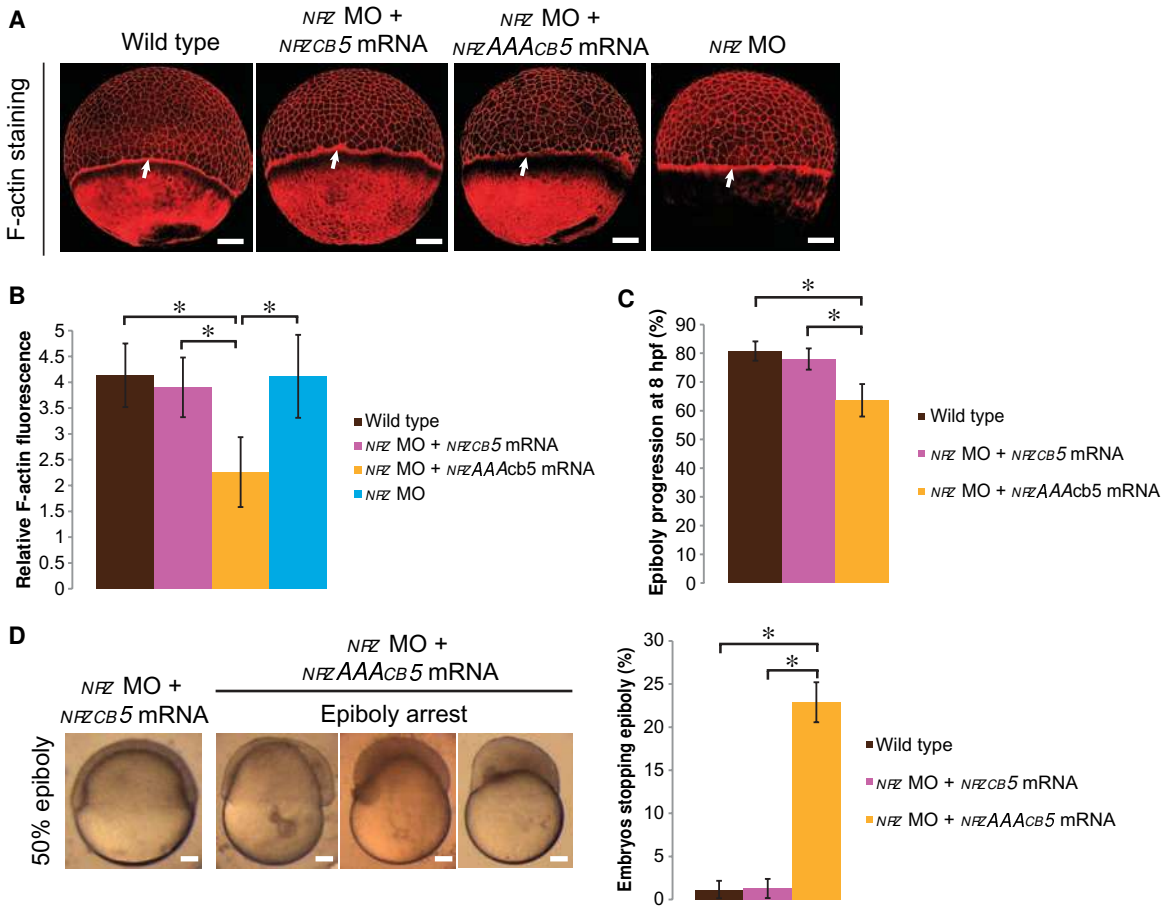


Fig. 8. Nrz phosphorylation is required for epiboly progression and actin ring formation. (**A**) Phalloidin-rhodamine staining of F-actin in embryos at the shield stage injected with *nrz* MO alone or in combination with *nrzcb5* or *nrzAAAcb5* mRNA. White arrows indicate the actin-myosin ring. (**B**) Histogram showing the relative actin fluorescence (mean ± SD). Relative fluorescence is indicative of the amount of F-actin at the blastoderm margin and was calculated by using the ratio of the rhodamine fluorescence at the blastoderm margin to the rhodamine fluorescence in the blastomeres. $n$ = 30 embryos per condition. (**C**) Histogram showing the mean percentage (±SD) of epiboly progression at 8 hours post-fertilization (hpf). $n$ = 90 embryos from 3 independent injections. (**D**) Representative images of the phenotypes (epiboly arrest) of embryos at 5 hpf injected with *nrz* MO and *nrzcb5* or *nrzAAAcb5* mRNA. NrzCb5 restores epiboly progression (50% epiboly), in contrast to NrzAAACb5 (epiboly arrest). $n$ = 3 independent injections (80 to 100 embryos per injection per condition). Scale bars, 20 μm. *$P$ < 0.005 (Mann-Whitney $U$ test) for (B) to (D).

waves during early epiboly could time MLC phosphorylation and the progressive assembly of the actin-myosin ring.

Our results identify the role of Nrz in IICR and emphasize the role of Bcl-2 family proteins in the regulation of intracellular $Ca^{2+}$. We recently demonstrated that Bcl-wav, a newly characterized Bcl-2 family member, is essential for convergence and extension movement in zebrafish gastrulation. During this process, Bcl-wav regulates the formation of actin protrusions via its role in mitochondrial $Ca^{2+}$ uptake (*37*). Together, these studies emphasize the diversity of functional roles of Bcl-2 family proteins in numerous cellular processes.

## MATERIALS AND METHODS

### MOs, reagents, and antibodies

The *nrz* MO was designed according to the manufacturer's recommendations (Gene Tools, LLC) and had the following sequence: 5′-CATTTTCCTCCCAGCGATGTCAGAC-3′. A second MO that contained four mismatches relative to *nrz* MO was used as a negative control (control MO). The sequence was as follows: 5′-CATTATCCTGCCAGCCATGTGAGAC-3′ (*13*).

The following antibodies were used: $IP_3R1$ (PA1-901, Thermo Scientific), rabbit FLAG (F-7425, Sigma-Aldrich), mouse FLAG (F-3165, Sigma-Aldrich), rabbit hemagglutinin (HA) (Ab75640, Abcam), mouse HA (MMS-101P, Covance), PARP (Ab6079, Abcam), vinculin (SC-55465, Santa Cruz Biotechnology), Bax (5023, Cell Signaling), and phosphoserine (05-1000, Millipore).

### Vector construction and mRNA in vitro transcription

The open reading frames of *nrz* and *zbax* were cloned into the pCS2+ expression vector as previously described (*13*). The transmembrane domain of Cb5 was cloned in pCS2+ as previously described (*14*). Mutants of Nrz were inserted between the Cla I and Xho I restriction sites in the pCS2+Cb5 or pCS2+ vectors. For cloning of *zip$_3$r1*, total RNA from

embryos was extracted using TRIzol reagent (Invitrogen) following the manufacturer's instructions, and complementary DNA (cDNA) was generated with a cDNA synthesis kit (iScript cDNA synthesis kit, Bio-Rad) with 500 ng of total RNA and gene-specific primers. An HA tag was added to the N terminus by polymerase chain reaction. Gene fragments corresponding to the $IP_3R1$ domains were amplified and cloned between the Cla I and Xho I or between the Eco RI and Xho I sites in pCS2+. pcDNA3.1-IRIS was provided by K. Mikoshiba (*25*). In vitro transcription for the different constructs was performed with the SP6 mMESSAGE mMACHINE kit according to the manufacturer's recommendations (Ambion).

### Zebrafish husbandry, manipulation, injection, and analysis

Zebrafish (crosses between AB and TU or between AB and TL strains) were raised and maintained according to standard procedures (*38*). Zebrafish embryos were grown in E3 medium (5 mM NaCl, 0.17 mM KCl, 0.33 mM $CaCl_2$, 0.33 mM $MgSO_4$, pH 7.6) at 28.5°C.

MO (0.5 mM) and mRNA (100 ng/ml) injections were performed between the one- and four-cell stages. Embryos were then observed every 15 min, and embryos showing margin constriction and cell detachment from the yolk were recorded as "embryos with a phenotype." Calcium Green-1 Dextran (Invitrogen) at 250 μM was injected at the 128-cell stage into the top of the yolk, close to the margin of the yolk and blastoderm.

Images of embryos at 8 hpf were acquired with a Nikon TE30 inverted microscope and MetaMorph software. Epiboly was quantified with Image J software by measuring the distance of the blastoderm margin from the animal pole (*D*) and the size of the embryos (*S*). Epiboly progression data were obtained by using the ratio *D*/*S*. F-actin staining of embryos was performed as previously described (*36*). In brief, embryos at the desired stage were fixed overnight in 4% paraformaldehyde at 4°C and washed in PBT [0.1% Triton-X 100 in phosphate-buffered saline (PBS)]. They were then permeabilized for 1 hour in 0.5% Triton-X in PBS and subsequently incubated in block solution (10% goat serum, 1% dimethyl sulfoxide, 0.1% Triton-X 100 in PBS) for 5 hours. The embryos were then incubated in rhodamine-phalloidin (Invitrogen) overnight at 4°C and washed three times in PBT.

Embryos used for $Ca^{2+}$ imaging were injected with Calcium Green-1 Dextran (Invitrogen) at 250 μM into the top of the yolk at the blastoderm margin of 128-cell stage embryos (*10*), dechorionated, and mounted in low–melting point 0.7% agarose in E3 medium on the stage of a Zeiss LSM 780 microscope and incubated at 28.5°C. Stacks of 4 μm were acquired, and the sum of the first three stacks was used to visualize variations in $Ca^{2+}$ concentration in the external YSL.

ER from the YSL was isolated as described previously (*14*). The 100,000*g* pellet was resuspended in TNE buffer [10 mM tris-HCl, 200 mM NaCl, 1 mM EDTA (pH 7.4), 1 mM β-glycerophosphate, 1 mM orthovanadate, 0.1 mM sodium pyrophosphate containing protease inhibitors] and was used for FLAG immunoprecipitation.

### Cell culture, immunoprecipitation, $Ca^{2+}$ imaging, and FRET

HeLa cells were grown in Dulbecco's modified Eagle's medium (high glucose) (Gibco) supplemented with 10% fetal bovine serum and 1% penicillin-streptomycin (Gibco) at 37°C in a 5% $CO_2$ humidified atmosphere.

For endogenous $IP_3R$ and Bax coimmunoprecipitation experiments, $6 \times 10^6$ HeLa cells were transfected with the indicated vectors. After 24 hours, cells were lysed in TNE buffer. Extracts were precleared with protein G–Sepharose beads for 1 hour at 4°C and then incubated overnight with 5 μg of $IP_3R$ or Bax primary antibody. The extracts were then incubated with protein G–Sepharose beads for 2 hours. Immunoprecipitated fractions were washed three times with TNE and analyzed by immunoblotting. For HA and FLAG immunoprecipitation, $1 \times 10^6$ HeLa cells were transfected with the indicated vectors and lysed and processed as above. One microgram of primary rabbit HA or rabbit FLAG was used.

For $Ca^{2+}$ imaging, HeLa cells cultured in Nunc Lab-Tek chambered cover glass were incubated with 5 μM FluoForte (Enzo Life Sciences) in a $Ca^{2+}$-free balanced salt solution (BSS) [121 mM NaCl, 5.4 mM KCl, 0.8 mM $MgCl_2$, 6 mM $NaHCO_3$, 5.5 mM D-glucose, 25 mM Hepes (pH 7.3)] for 1 hour at 37°C. Fluorescence values were collected using a Zeiss LSM 780 confocal microscope. After 10 s of measurement, 5 μM histamine (Sigma) or thapsigargin (Enzo Life Sciences) in $Ca^{2+}$-free BSS was injected. For IRIS FRET, HeLa cells cultured in Nunc Lab-Tek chambered cover glass were cotransfected with pcDNA3.1-IRIS (*25*) and pCS2+ encoding the various Nrz mutants ($n_{mole}$ ratio, 1:3). Before imaging, the medium was replaced with BSS. FRET was measured with a Zeiss LSM 780 confocal microscope by excitation at 405 nm. ECFP and Venus fluorescence were detected at 450 to 510 nm and 525 to 565 nm, respectively. After 10 s of measurement, 5 μM histamine in BSS was injected. Changes in the FRET signal were calculated using the $F_{ECFP}/F_{Venus}$ ratio (*R*).

### $IP_3$-FITC fluorescence polarization measurement

$IP_3$-FITC, $IP_3$, and the recombinant N-terminal domain protein were purchased with the HitHunter $IP_3$ assay kit from DiscoveRx. Recombinant Nrz protein was produced as previously described (*13*). $IP_3$-FITC at 0.5 nM was incubated with 4 nM of recombinant NTD and the various recombinant Nrz proteins for 30 min at 25°C. Fluorescence polarization was recorded at 25°C with 485-nm excitation and 530-nm emission filters, using a Mithras LB 940 multimode microplate reader (Berthold Technologies).

### Sequence alignment

Nrz ortholog sequences were found in the National Center for Biotechnology Information protein database. Sequence alignment was performed with the Clustal Omega tool at http://www.ebi.ac.uk/Tools/msa/clustalo/. An image of the alignment was obtained with Jalview software (*39*).

### Molecular docking simulation

The Nrz protein structure was obtained by analyzing the Nrz amino acid sequence on the Phyre$^2$ (*40*) homology modeling server. The Nrz BH4 domain structure was extracted, and a docking experiment was performed against the $IP_3R1$ binding domain crystal structure (PDB: 1N4K) using the PatchDock server (*41*). Images were acquired with UCSF Chimera software (*42*).

### Statistical analysis

Statistical significance was analyzed using the Mann-Whitney *U* test; $P < 0.005$ was considered significant.

### SUPPLEMENTARY MATERIALS

www.sciencesignaling.org/cgi/content/full/7/312/ra14/DC1

List of primers

Fig. S1. Sequence alignment of the BH4 domains of Nrz, zBcl-2, and zBcl-xL.

Fig. S2. Interaction of Nrz with $IP_3BD$ requires the BH4 domain.

Fig. S3. Sequence alignment of the BH4 domains of Nrz orthologs.

Fig. S4. Nrz does not reduce the ER $Ca^{2+}$ content.

Movie S1. $Ca^{2+}$ waves in the YSL of a wild-type uninjected embryo.

Movie S2. $Ca^{2+}$ waves in the YSL of an *nrzcb5*-injected embryo.

Movie S3. $Ca^{2+}$ waves in the YSL of an *nrzAAAcb5*-injected embryo.

## REFERENCES AND NOTES


1. R. J. Youle, A. Strasser, The BCL-2 protein family: Opposing activities that mediate cell death. *Nat. Rev. Mol. Cell Biol.* **9**, 47–59 (2008).
2. B. Bonneau, J. Prudent, N. Popgeorgiev, G. Gillet, Non-apoptotic roles of Bcl-2 family: The calcium connection. *Biochim. Biophys. Acta* **1833**, 1755–1765 (2013).
3. K. Uchida, H. Miyauchi, T. Furuichi, T. Michikawa, K. Mikoshiba, Critical regions for activation gating of the inositol 1,4,5-trisphosphate receptor. *J. Biol. Chem.* **278**, 16551–16560 (2003).
4. I. Bosanac, T. Michikawa, K. Mikoshiba, M. Ikura, Structural insights into the regulatory mechanism of $IP_3$ receptor. *Biochim. Biophys. Acta* **1742**, 89–102 (2004).
5. Y. P. Rong, A. S. Aromolaran, G. Bultynck, F. Zhong, X. Li, K. McColl, S. Matsuyama, S. Herlitze, H. L. Roderick, M. D. Bootman, G. A. Mignery, J. B. Parys, H. De Smedt, C. W. Distelhorst, Targeting Bcl-2-$IP_3$ receptor interaction to reverse Bcl-2's inhibition of apoptotic calcium signals. *Mol. Cell* **31**, 255–265 (2008).
6. C. White, C. Li, J. Yang, N. B. Petrenko, M. Madesh, C. B. Thompson, J. K. Foskett, The endoplasmic reticulum gateway to apoptosis by Bcl-$X_L$ modulation of the $InsP_3R$. *Nat. Cell Biol.* **7**, 1021–1028 (2005).
7. M. J. Berridge, P. Lipp, M. D. Bootman, The versatility and universality of calcium signalling. *Nat. Rev. Mol. Cell Biol.* **1**, 11–21 (2000).
8. O. Markova, P. F. Lenne, Calcium signaling in developing embryos: Focus on the regulation of cell shape changes and collective movements. *Semin. Cell Dev. Biol.* **23**, 298–307 (2012).
9. C. B. Kimmel, W. W. Ballard, S. R. Kimmel, B. Ullmann, T. F. Schilling, Stages of embryonic development of the zebrafish. *Dev. Dyn.* **203**, 253–310 (1995).
10. M. Y. F. Yuen, S. E. Webb, C. M. Chan, B. Thisse, C. Thisse, A. L. Miller, Characterization of $Ca^{2+}$ signaling in the external yolk syncytial layer during the late blastula and early gastrula periods of zebrafish development. *Biochim. Biophys. Acta* **1833**, 1641–1656 (2013).
11. S. E. Webb, A. L. Miller, Calcium signalling during embryonic development. *Nat. Rev. Mol. Cell Biol.* **4**, 539–551 (2003).
12. M. Behrndt, G. Salbreux, P. Campinho, R. Hauschild, F. Oswald, J. Roensch, S. W. Grill, C. P. Heisenberg, Forces driving epithelial spreading in zebrafish gastrulation. *Science* **338**, 257–260 (2012).
13. E. Arnaud, K. F. Ferri, J. Thibaut, Z. Haftek-Terreau, A. Aouacheria, D. Le Guellec, T. Lorca, G. Gillet, The zebrafish bcl-2 homologue Nrz controls development during somitogenesis and gastrulation via apoptosis-dependent and -independent mechanisms. *Cell Death Differ.* **13**, 1128–1137 (2006).
14. N. Popgeorgiev, B. Bonneau, K. F. Ferri, J. Prudent, J. Thibaut, G. Gillet, The apoptotic regulator Nrz controls cytoskeletal dynamics via the regulation of $Ca^{2+}$ trafficking in the zebrafish blastula. *Dev. Cell* **20**, 663–676 (2011).
15. Y. P. Rong, G. Bultynck, A. S. Aromolaran, F. Zhong, J. B. Parys, H. De Smedt, G. A. Mignery, H. L. Roderick, M. D. Bootman, C. W. Distelhorst, The BH4 domain of Bcl-2 inhibits ER calcium release and apoptosis by binding the regulatory and coupling domain of the IP3 receptor. *Proc. Natl. Acad. Sci. U.S.A.* **106**, 14397–14402 (2009).
16. G. Monaco, E. Decrock, H. Akl, R. Ponsaerts, T. Vervliet, T. Luyten, M. De Maeyer, L. Missiaen, C. W. Distelhorst, H. De Smedt, J. B. Parys, L. Leybaert, G. Bultynck, Selective regulation of $IP_3$-receptor-mediated $Ca^{2+}$ signaling and apoptosis by the BH4 domain of Bcl-2 versus Bcl-Xl. *Cell Death Differ.* **19**, 295–309 (2012).
17. T. A. Brock, E. A. Capasso, Thrombin and histamine activate phospholipase C in human endothelial cells via a phorbol ester-sensitive pathway. *J. Cell. Physiol.* **136**, 54–62 (1988).
18. X. M. Yin, Z. N. Oltvai, S. J. Korsmeyer, BH1 and BH2 domains of Bcl-2 are required for inhibition of apoptosis and heterodimerization with Bax. *Nature* **369**, 321–323 (1994).
19. E. F. Eckenrode, J. Yang, G. V. Velmurugan, J. K. Foskett, C. White, Apoptosis protection by Mcl-1 and Bcl-2 modulation of inositol 1,4,5-trisphosphate receptor-dependent $Ca^{2+}$ signaling. *J. Biol. Chem.* **285**, 13678–13684 (2010).
20. G. Monaco, M. Beckers, H. Ivanova, L. Missiaen, J. B. Parys, H. De Smedt, G. Bultynck, Profiling of the Bcl-2/Bcl-$X_L$-binding sites on type 1 $IP_3$ receptor. *Biochem. Biophys. Res. Commun.* **428**, 31–35 (2012).
21. I. Bosanac, J. R. Alattia, T. K. Mal, J. Chan, S. Talarico, F. K. Tong, K. I. Tong, F. Yoshikawa, T. Furuichi, M. Iwai, T. Michikawa, K. Mikoshiba, M. Ikura, Structure of the inositol 1,4,5-trisphosphate receptor binding core in complex with its ligand. *Nature* **420**, 3–7 (2002).
22. H. Ando, A. Mizutani, T. Matsu-ura, K. Mikoshiba, IRBIT, a novel inositol 1,4,5-trisphosphate ($IP_3$) receptor-binding protein, is released from the $IP_3$ receptor upon $IP_3$ binding to the receptor. *J. Biol. Chem.* **278**, 10602–10612 (2003).
23. H. Ando, A. Mizutani, H. Kiefer, D. Tsuzurugi, T. Michikawa, K. Mikoshiba, IRBIT suppresses $IP_3$ receptor activity by competing with $IP_3$ for the common binding site on the $IP_3$ receptor. *Mol. Cell* **22**, 795–806 (2006).
24. C. J. Hanson, M. D. Bootman, C. W. Distelhorst, R. J. H. Wojcikiewicz, H. L. Roderick, Bcl-2 suppresses $Ca^{2+}$ release through inositol 1,4,5-trisphosphate receptors and inhibits $Ca^{2+}$ uptake by mitochondria without affecting ER calcium store content. *Cell Calcium* **44**, 324–338 (2008).
25. T. Matsu-ura, T. Michikawa, T. Inoue, A. Miyawaki, M. Yoshida, K. Mikoshiba, Cytosolic inositol 1,4,5-trisphosphate dynamics during intracellular calcium oscillations in living cells. *J. Cell Biol.* **173**, 755–765 (2006).
26. A. M. Rossi, C. W. Taylor, Analysis of protein-ligand interactions by fluorescence polarization. *Nat. Protoc.* **6**, 365–387 (2011).
27. M. C. Bassik, L. Scorrano, S. A. Oakes, T. Pozzan, S. J. Korsmeyer, Phosphorylation of BCL-2 regulates ER $Ca^{2+}$ homeostasis and apoptosis. *EMBO J.* **23**, 1207–1216 (2004).
28. J. C. Cheng, A. L. Miller, S. E. Webb, Organization and function of microfilaments during late epiboly in zebrafish embryos. *Dev. Dyn.* **231**, 313–323 (2004).
29. J. M. Vicencio, C. Ortiz, A. Criollo, A. W. Jones, O. Kepp, L. Galluzzi, N. Joza, I. Vitale, E. Morselli, M. Tailler, M. Castedo, M. C. Maiuri, J. Molgó, G. Szabadkai, S. Lavandero, G. Kroemer, The inositol 1,4,5-trisphosphate receptor regulates autophagy through its interaction with Beclin 1. *Cell Death Differ.* **16**, 1006–1017 (2009).
30. S. Zhang, S. Malmersjö, J. Li, H. Ando, O. Aizman, P. Uhlén, K. Mikoshiba, A. Aperia, Distinct role of the N-terminal tail of the Na,K-ATPase catalytic subunit as a signal transducer. *J. Biol. Chem.* **281**, 21954–21962 (2006).
31. A. Miyakawa-Naito, P. Uhlén, M. Lal, O. Aizman, K. Mikoshiba, H. Brismar, S. Zelenin, A. Aperia, Cell signaling microdomain with Na,K-ATPase and inositol 1,4,5-trisphosphate receptor generates calcium oscillations. *J. Biol. Chem.* **278**, 50355–50361 (2003).
32. J. Hirota, H. Ando, K. Hamada, K. Mikoshiba, Carbonic anhydrase-related protein is a novel binding protein for inositol 1,4,5-trisphosphate receptor type 1. *Biochem. J.* **372**, 435–441 (2003).
33. L. Scorrano, S. A. Oakes, J. T. Opferman, E. H. Cheng, M. D. Sorcinelli, T. Pozzan, S. J. Korsmeyer, BAX and BAK regulation of endoplasmic reticulum $Ca^{2+}$: A control point for apoptosis. *Science* **300**, 135–139 (2003).
34. M. B. Ferrari, J. Rohrbough, N. C. Spitzer, Spontaneous calcium transients regulate myofibrillogenesis in embryonic *Xenopus* myocytes. *Dev. Biol.* **178**, 484–497 (1996).
35. H. Li, J. D. Cook, M. Terry, N. C. Spitzer, M. B. Ferrari, Calcium transients regulate patterned actin assembly during myofibrillogenesis. *Dev. Dyn.* **229**, 231–242 (2004).
36. M. Köppen, B. G. Fernández, L. Carvalho, A. Jacinto, C. P. Heisenberg, Coordinated cell-shape changes control epithelial movement in zebrafish and *Drosophila*. *Development* **133**, 2671–2681 (2006).
37. J. Prudent, N. Popgeorgiev, B. Bonneau, J. Thibaut, R. Gadet, J. Lopez, P. Gonzalo, R. Rimokh, S. Manon, C. Houart, P. Herbomel, A. Aouacheria, G. Gillet, Bcl-wav and the mitochondrial calcium uniporter drive gastrula morphogenesis in zebrafish. *Nat. Commun.* **4**, 2330 (2013).
38. M. Westerfield, *A Guide for the Laboratory Use of Zebrafish (Danio rerio)* (University of Oregon Press, Eugene, OR, ed. 3, 1995).
39. A. M. Waterhouse, J. B. Procter, D. M. A. Martin, M. Clamp, G. J. Barton, Jalview Version 2—A multiple sequence alignment editor and analysis workbench. *Bioinformatics* **25**, 1189–1191 (2009).
40. L. A. Kelley, M. J. E. Sternberg, Protein structure prediction on the Web: A case study using the Phyre server. *Nat. Protoc.* **4**, 363–371 (2009).
41. D. Schneidman-Duhovny, Y. Inbar, R. Nussinov, H. J. Wolfson, PatchDock and SymmDock: Servers for rigid and symmetric docking. *Nucleic Acids Res.* **33**, W363–W367 (2005).
42. E. F. Pettersen, T. D. Goddard, C. C. Huang, G. S. Couch, D. M. Greenblatt, E. C. Meng, T. E. Ferrin, UCSF Chimera—A visualization system for exploratory research and analysis. *J. Comput. Chem.* **25**, 1605–1612 (2004).



**Acknowledgments:** We thank K. Mikoshiba for providing the IRIS construct and S. Chabaud (UBET, Centre Léon Bérard), C. Vanbelle (CeCILE—SFR Santé Lyon-Est), and C. Bouchardon (CeCILE—SFR Santé Lyon-Est) for their technical assistance. **Funding:** This work was supported by AFMTéléthon, Ligue nationale contre le cancer (comité de la Drôme), Fondation ARC pour la recherche sur le cancer. B.B. and A.N. are fellows of the Ministère de la Recherche. N. Peyriéras received support from France BioImaging ANR-10-INBS-04 (BioEmergences platform). **Author contributions:** B.B., A.N., J.P., and N. Popgeorgiev performed the experiments. B.B., N. Peyriéras, R.R., and G.G. designed the experiments. B.B. and G.G. wrote the manuscript. **Competing interests:** The authors declare that they have no competing interests.